Subdermal Flexible Solar Cell Arrays for Powering Medical Electronic Implants

Kwangsun Song, Jung Hyun Han, Taehoon Lim, Namyun Kim, Sungho Shin, Juho Kim, Hyuck Choo, Sungho Jeong, Yong-Chul Kim, Zhong Lin Wang, and Jongho Lee*

As the average lifespan increases, people have more chances to rely on implantable electronic devices[1,2] to monitor abnormal biosignals, such as insertable cardiac monitors (ICMs), or to assist malfunctioning organs, such as pacemakers, spinal cord stimulators, vagus nerve stimulators, or deep brain stimulators.[3] In addition, increased demand for new biomedical applications increases development of new types of implants, such as blood pressure monitors,[4] glucose monitors,[5] artificial retinas,[6] and related research.[7–12] All of these implantable medical devices require electrical power to function within the body. However, these devices usually use integrated batteries whose electrical capacities are limited. For example, pacemaker batteries usually lasts 5 to 8 years and requires additional surgeries to periodically replace the modules.[2] Pacemakers are one of the widely used implantable electronics and more than 20% of the implant is for reintervention.[1] Various innovative approaches are being actively developed for power in vivo devices, using electrochemical reactions,[13,14] mechanical movement,[15–18] wireless power transfer,[19–22] and others,[23]

K. Song, T. Lim, N. Kim, S. Shin, J. Kim,
Prof. S. Jeong, Prof. J. Lee
School of Mechanical Engineering
Gwangju Institute of Science and Technology (GIST)
Gwangju 500-712, South Korea
E-mail: jong@gist.ac.kr
K. Song, J. Kim, Prof. J. Lee
Research Institute for Solar and Sustainable Energies
Gwangju Institute of Science and Technology (GIST)
Gwangju 500-712, South Korea
Dr. J. H. Han, Prof. Y.-C. Kim
Department of Medical System Engineering
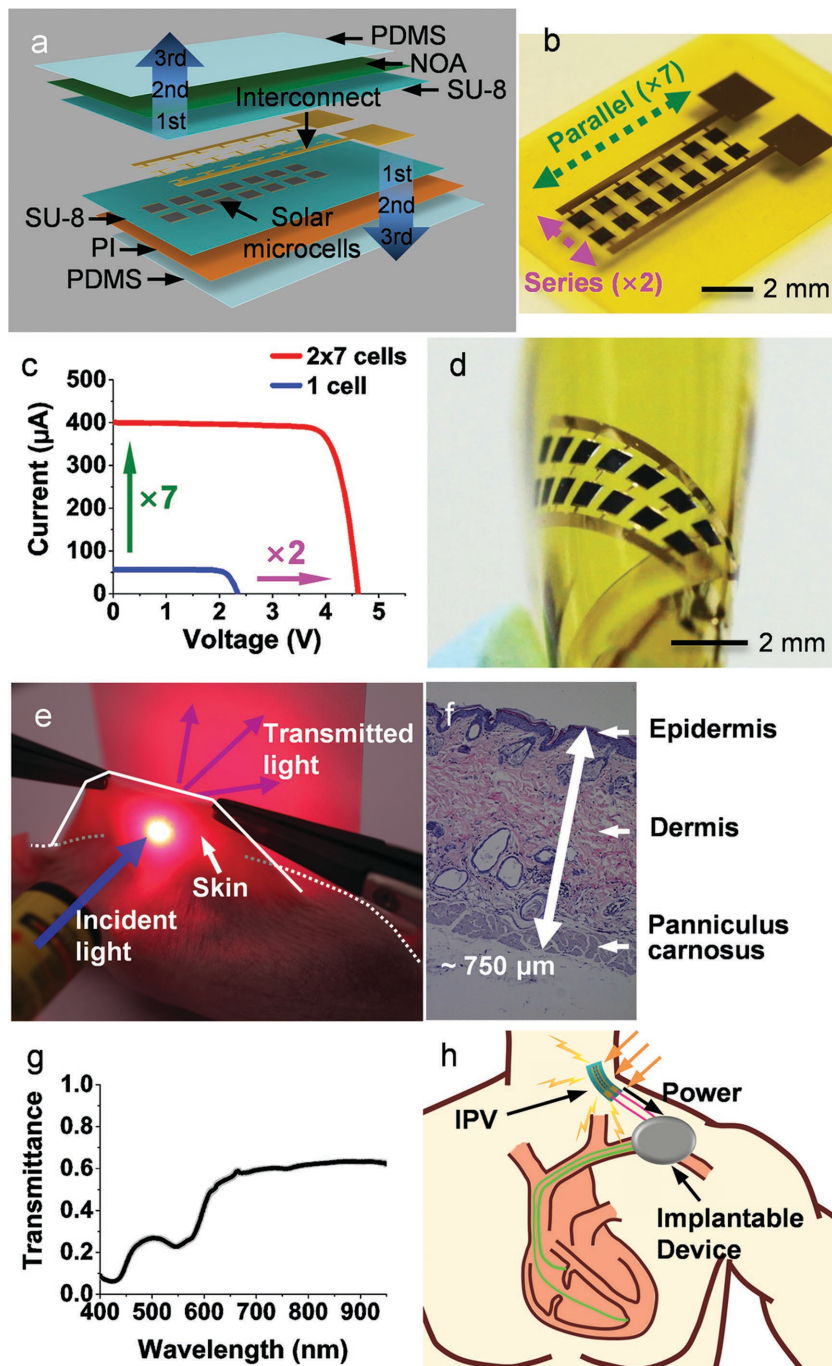Gwangju Institute of Science and Technology (GIST)
Gwangju 500-712, South Korea
Prof. H. Choo
Department of Electrical Engineering
California Institute of Technology
Pasadena, CA 91125, USA
Prof. H. Choo
Department of Medical Engineering
California Institute of Technology
Pasadena, CA 91125, USA
Prof. Y.-C. Kim
School of Life Science
Gwangju Institute of Science and Technology (GIST)
Gwangju 500-712, South Korea
Prof. Z. L. Wang
School of Materials Science and Engineering
Georgia Institute of Technology
Atlanta, GA 30332, USA

with aims of overcoming limitations[24,25] associated with the amount of energy generated in vivo, biocompatibility or durability. Recent results using biofuel cells based on electrochemical reaction report attractive technologies to power in vivo biomedical devices using abundant sources such as blood, sweat or tear in living things.[26–30] In addition, recently, researchers also investigated the use of silicon photodiodes for a retinal prosthesis in ocular globes,[31,32] and silicon solar cells for a pacemaker.[33,34] These promising approaches take the advantage of the transparency or translucency of live tissues with relatively stiff or rigid devices. However, photovoltaics in more flexible forms are highly desired for use in biomedical applications to avoid tissue stress, patient discomfort, or even skin perforation in some cases. Here, we describes an approach to harvest higher levels of energy in vivo by using flexible and implantable forms of ultrathin photovoltaic devices that are transfer-assembled and encapsulated with biocompatible materials to subdermally capture transmitted light through the skin and generate DC electricity. When used in live hairless mouse models, the implanted photovoltaic (IPV) devices generated approximately 647 µW of direct current power, which is significantly higher than previously reported.[13–18,23] As a proof of concept for a fully implantable IPV device, we report the results of an IPV device that was integrated with a custom-built flexible pacemaker and a rechargeable battery. This system was then implanted into a live hairless mouse, and electricity directly generated or stored by the IPV device operated the pacemaker. Direct and indirect biocompatibility assessments ensure that encapsulation layers prevent toxic elements from leaching to the surrounding tissues. Our technology may provide an alternative approach for powering in vivo medical devices and for extending battery life with extra power whenever possible, with a broad range of applications.

The thin film based flexible solar cell arrays were fabricated using existing technologies.[35] **Figure 1**a shows an exploded view of the IPV device in which sputtered metals (Ti: 30 nm/Au: 300 nm) interconnect the array of ultrathin dual-junction solar microcells (size: 760 µm × 760 µm, thickness: 5.7 µm, GaInP/GaAs) that is transfer-printed on the flexible polyimide film (PI, thickness: 12.5 µm). Specific details are in the Experimental Section. The interconnected devices are encapsulated with multiple layers of biocompatible,[36–38] transparent[39–41] polymers, such as SU-8 (≈2 µm, SU-8 2002, Microchem), Norland optical adhesive (≈23 µm, NOA 61, Norland Products) and polydimethylsiloxane (PDMS, 100–200 µm, Sylgard 184, Dow Corning). This relatively simple design provides a thin and flexible structure to be more mechanically compatible with skin. Figure 1b shows the representative unencapsulated image

**ADVANCED
HEALTHCARE
MATERIALS**

www.advhealthmat.de

COMMUNICATION

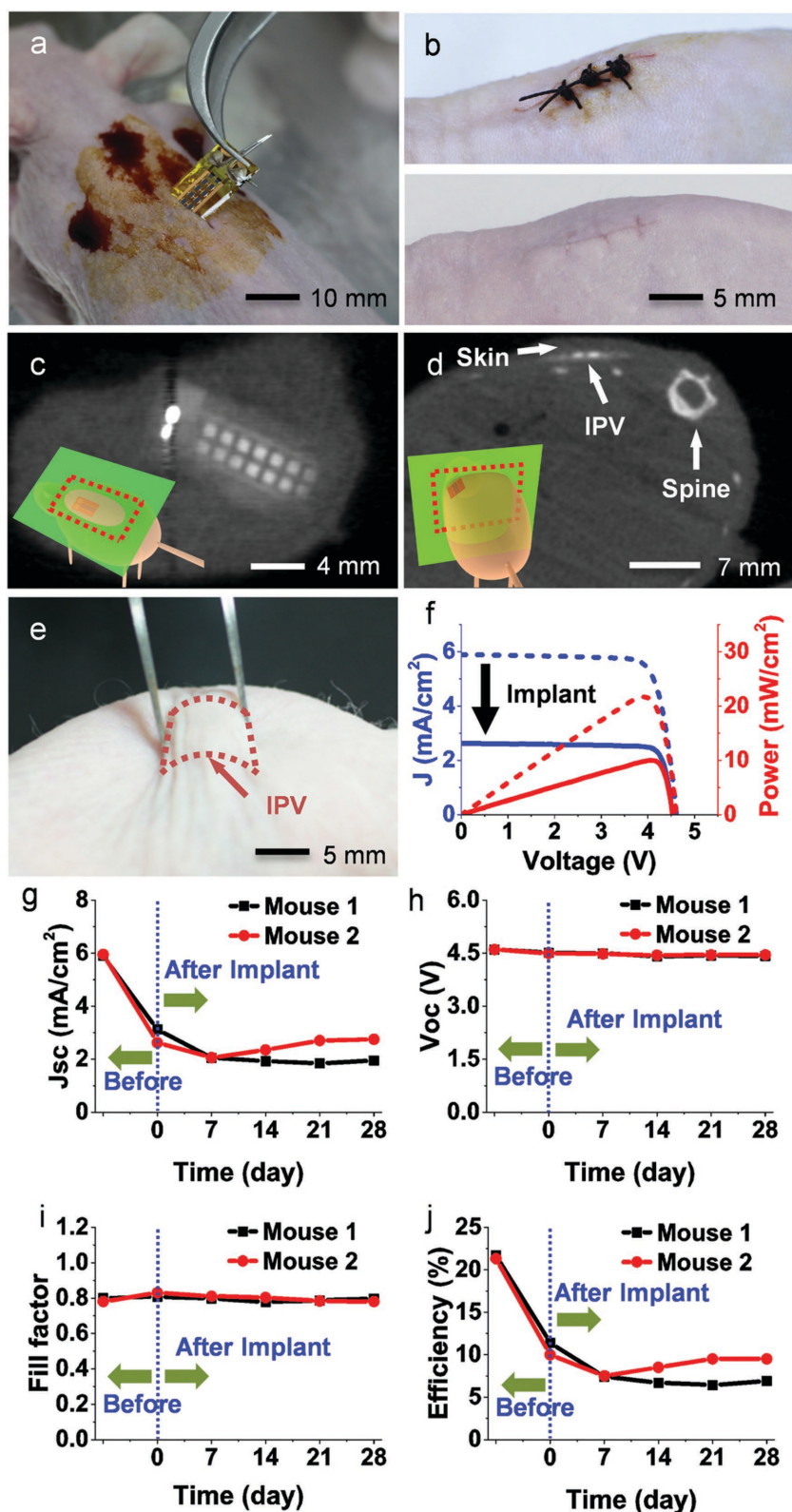*Materials Views*

www.MaterialsViews.com

Figure 1. Subdermal implantable photovoltaic (IPV) devices and optical properties of skins.
a) A schematic illustration of an IPV device in a tilted, exploded view. Thicknesses of the encapsulation layers were optimized to minimize strain to the solar microcells and metal interconnections. b) An optical image of the fabricated IPV device. Thin metal layers (Ti: 20 nm, Au: 300 nm) interconnect seven solar microcells in parallel and two solar microcells in series to generate desired current and voltage. c) Current and voltage characteristics of single and interconnected solar microcells. Parallel and series interconnections increase short circuit current seven times (I_{sc}: 57 µA → 400 µA) and open circuit voltage two times (V_{oc}: 2.3 V → 4.6 V), respectively. Fill factor and power conversion efficiency of the IPV device are 0.8% and 21.7%, respectively. d) An image of the IPV device in bending. e) Demonstration of light (wavelength ≈532 nm) transmission through skin of a live hairless mouse (SKH1-Hr[hr]). f) A histological microscope image of the skin (epidermis ≈50 µm, dermis ≈600 µm, panniculus carnosus ≈100 µm). g) Transmittance (mean ± SEM) of skins, measured within 10 min after isolating from seven live hairless mice (total 28 skins, 4 skins from each mouse). Transmittance is about 20%–40% at

consisting of 14 solar microcells, 7 columns interconnected in parallel, and 2 rows in series. The interconnections improved short-circuit current seven times (I_{sc}: 57 µA → 400 µA) and open-circuit voltage two times (V_{oc}: 2.3 V → 4.6 V) as shown in the current–voltage characteristics in Figure 1c. The IPV device, designed to reduce strain on the brittle solar microcells and metal interconnections (Figures S2 and S3, Supporting Information), is mechanically flexible as shown in Figure 1d. Current–voltage characteristics remain the same after bending the IPV device on a cylinder with a radius as small as 1.75 mm (Figure S4, Supporting Information). Conversion efficiency and power density remain without noticeable degradation even after more than 1000 repetitive cycling tests on a cylinder with a radius of 2.5 mm (Figure S5, Supporting Information).

Figure 1e demonstrates the translucence of skin by showing the incident and transmitted light (≈532 nm) through a dorsal skinfold of a live hairless mouse (SKH1-Hr[hr]), which is commonly used in dermatologic research as a substitute for human skin.[42] The transmitted light is able to illuminate a white paper on the other side of the skin. This observation inspired us to use light as a medium to deliver energy through the skin to power various electrical implants without invasive wires that can be a source of infection.[43] Prolonged percutaneous medical device is well known as a source of infection as a passage of microorganisms.[44] Figure 1f shows a cross-sectional image of skin, consisting of epidermis (≈50 µm), dermis (≈600 µm), and panniculus carnosus (≈100 µm) of the hairless mouse. Measurements of the optical properties of skin isolated from seven live mice (total 28 skins, 4 skins from each mouse) within 10 min (see the Experimental Section) reveal that about 20%–40% of an incident light of 450–600 nm and about 50%–60% of an incident light of 600–950 nm can pass through the skin (Figure 1g). Although the skins limit the transmittance, several tens of percent of the incident light can be utilized to generate electricity. Subdermal IPV devices can capture the transmitted light and generate electricity to sustainably power implantable devices in the body, such as a pacemaker, as illustrated in Figure 1h.

relatively lower wavelengths (450–600 nm) and about 50%–60% at higher wavelengths (600–950 nm). h) A schematic illustration of a potential application of the IPV devices that power implantable electronic devices such as a pacemaker.

Makerials Views

www.MaterialsViews.com

ADVANCED
HEALTHCARE
MATERIALS

www.advhealthmat.de

COMMUNICATION

Figure 2. Surgical procedures and electrical performances of the subdermal IPV devices in vivo. a) An optical image during surgical procedure to implant the IPV device under the back skin of a hairless mouse. The copper wires only for in vivo measurements of electrical performances can be removed through another simple procedure. b) Images of the surgical scar after stitching (upper) and after healing (lower). c,d) CT scans (c) parallel and (d) perpendicular to the IPV

To demonstrate the in vivo electrical performances, IPV devices were implanted into live mouse models. The surgery begins with a straight incision (≈10 mm) on the back of the hairless mouse under general anesthesia. The adipose (fat) layer under panniculus carnosus is separated by inserting iris scissors. **Figure 2**a shows an IPV device being implanted with copper wires (radius: 0.1 mm) that are only used to measure in vivo electrical characteristics. Figure 2b (upper) is post-surgery, and Figure 2b (lower) shows the incision healing within 2 weeks. See details in the Experimental Section. The computerized tomography (CT) scan images, taken 2 weeks after surgery, show the settled IPV device under the skin in Figure 2c,d. Designed to be durable even after cyclic bending tests on a cylinder with a radius of 1.75 mm (FEM, in Figure S3, Supporting Information), the IPV devices bend without breaking even after external loads are applied, for example, by pinching (radius of curvature ≈4 mm) as shown in Figure 2e.

Figure 2f shows the current–voltage and power characteristics of the IPV device prior to (dashed lines, in standard test condition, AM1.5G, 100 mW cm^{-2}) and after (solid lines, under the skin) surgery. Reduced light intensity under the skin results in decreased short-circuit current density (J_{sc}) from 5.9 to 2.6 mA cm^{-2}, maximum power density (Pmax) from 22 to 10 mW cm^{-2}, and conversion efficiency (η) from 21.7% to 10%. Open-circuit voltage (V_{oc}) and fill factor (FF) that depend on physical properties of the PV materials[45] remain constant (V_{oc}: 4.5 V, FF: 0.80–0.83). Long-term electrical performances are an important consideration for reliable usage of IPV devices in bodies. The electrical characteristics of two IPV devices implanted in two separate live hairless mice were measured every week for 4 weeks as shown in Figure 2g–j.

device implanted in a live mouse model. e) An image of pinching the subdermal IPV device. f) Current–voltage characteristic of the IPV device measured in vivo, before (dashed lines) and right after (solid lines) the surgery. g–j) In vivo measurement results of electrical performances of the subdermal IPV devices in two live mouse models for 4 weeks. g) J_{sc} reduces to 2.04 mA cm^{-2} for both mouse 1 (black square) and mouse2 (red circle) in a week. After 1 week, J_{sc} for mouse 1 decreases slightly (1.94 mA cm^{-2}) but J_{sc} for mouse 2 increases up to 2.75 mA cm^{-2} until both reach plateau at 3 weeks. h,i) V_{oc} and FF remain constant (V_{oc}: 4.5 V, FF: 0.80–0.83) for the two mice over 4 weeks, the conversion efficiency (η) changes similarly with J_{sc}, reaching plateau 6.9% for mouse 1 and 9.5% for mouse 2.

ADVANCED
HEALTHCARE
MATERIALS
www.advhealthmat.de

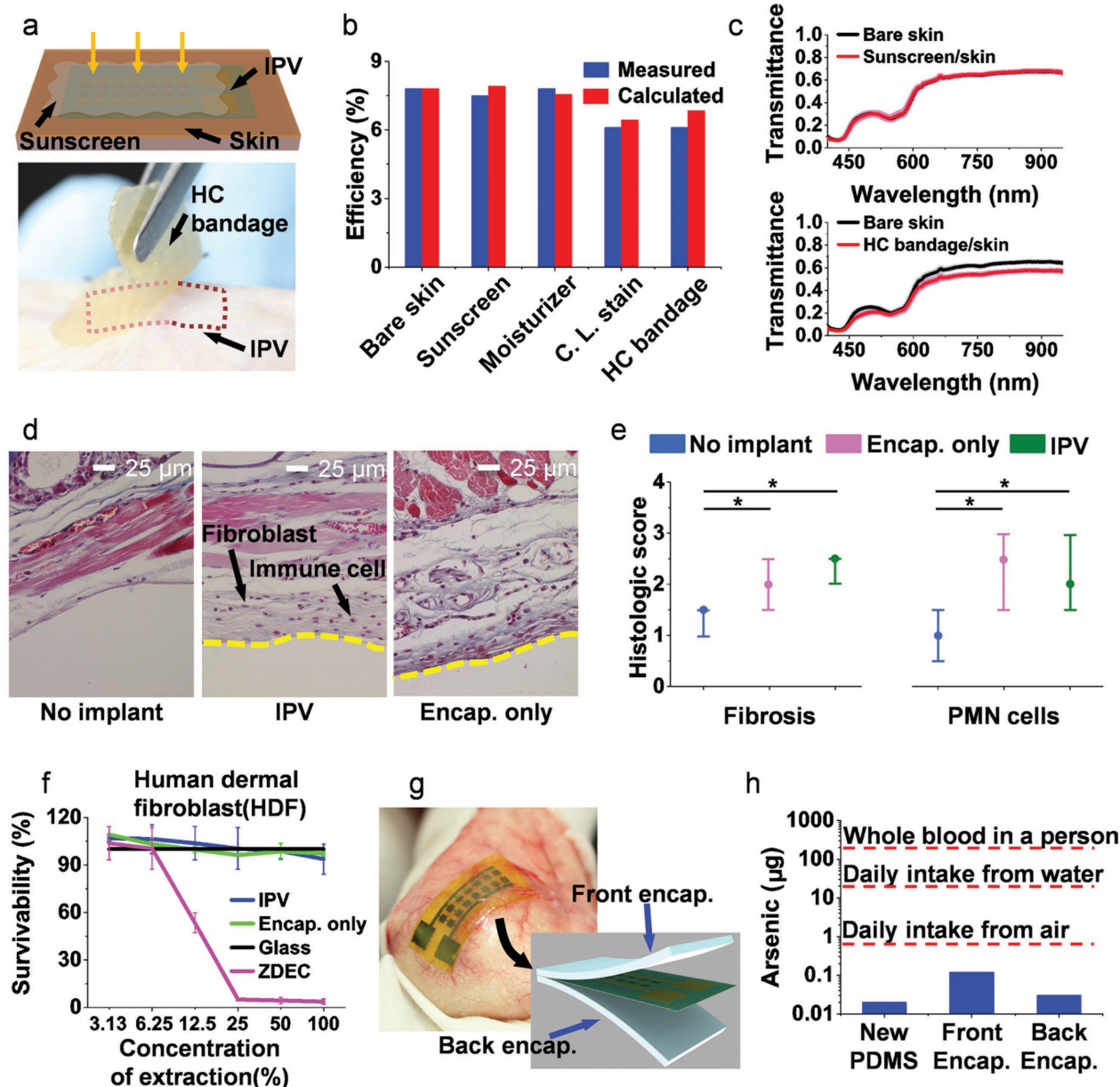Materials
Views
www.MaterialsViews.com

COMMUNICATION

In such a way, we were able to monitor changes of the electrical characteristics for each mouse (mouse1 and mouse2) over time. The J_{sc} (Figure 2g) of the mouse1 (black square) and mouse2 (red circle) decreased to 2.04 mA cm^{-2} 1 week after implantation and reached a plateau around 2 and 2.7 mA cm^{-2} at 3 weeks, respectively. V_{oc} and FF remain almost constant (V_{oc}: 4.5 V, FF: 0.80–0.83) over 4 weeks as in Figure 2h–i. Energy conversion efficiency (η) showing similar trends with J_{sc} drops to 7.5% for both mice in a week and reaches a plateau (6.7% for mouse1 and 9.5% for mouse2) around 3 weeks. Variations of the J_{sc} and η after implantation are attributed to differences in the skin thickness of each mouse, and the degree of immune response to the IPV devices affected the thickness of the skin, which can be surrounded by fibroblasts and immune cells.[46] Measurements of skinfold thicknesses around the implanted IPV devices for the mice at 5 weeks indicate that the skin of mouse1 ($\approx$675 µm) is about 136 µm thicker than that of mouse2 ($\approx$539 µm), resulting in lower current density and conversion efficiency. Although variations occur within 3 weeks after implantation, the electrical characteristics of the IPV devices stabilized after the third week. The results agree with other studies reporting that device interaction with surrounding tissues stabilized within 3 weeks.[47,48]

Additional coverings on the skin over the IPV device (as shown in **Figure 3**a) can lower conversion efficiencies. However, a layer of sunscreen (η = 7.5%, UV shield sun protector SPF 50+/PA+++) for protection against sunburn does not degrade electrical performance (η = 7.8% for bare skin) from in vivo measurements (blue bars as shown in Figure 3b) because sunscreens are usually designed to block ultraviolet rays (wavelength: 280–400 nm)[49] and minimally affect the transmittance of visible light (Figure 3c) that the IPV devices absorb. Calculated efficiencies (red bar in Figure 3b and Figure S7, Supporting Information) based on the reduced transmittance (Figure 3c and Figure S8, Supporting Information) by the additional layers predict the measured efficiencies well. More details for the coverings are shown in Table S1 of the Supporting Information.

Biocompatibility and cytotoxicity of the IPV devices are critically important for practical applications. Figure 3d shows the histology of three different tissues 4 weeks after implantation: with no implant, with the IPV device including the encapsulation layers, and with the encapsulation layers lacking the solar microcells (Figure S10, Supporting Information). For mice in 1–6 months old, developments are much faster ($\approx$45 times) than humans[50] and many studies described observation for 4 weeks to evaluate immune response of subcutaneous implantations in rodents.[51–53] More preparation details are in the Experimental Section. Both the IPV device and the encapsulation-only increased the number of fibroblasts and the number of immune cells. Histology analysis does not show significant differences between the IPV device and encapsulation-only. Histologic score of fibrosis for the IPV device (Median (interquartile range: 25%–75%) = 2.5 (2.0–2.5)) is comparable with that of the encapsulation-only (2.0 (1.5–2.5)) as in Figure 3e. Histologic scores of PMN cells for both the IPV device (2.0 (1.5–3.0)) and encapsulation only (2.5 (1.5–3.0)) are also comparable, demonstrating minimal effects of the solar microcells on the surrounding tissues. The histology analysis and histologic scores on the encapsulation layers are not more than expected.[53–55]

For clinical applications, long-term tissue damage assessments are also very important. More details are in the Experimental Section. To evaluate cytotoxicity of the IPV devices, we used human dermal fibroblasts (HDF) and splenocytes as surrogates for fibroblasts and immune cells, respectively, in surrounding tissues. Figure 3f shows cytotoxicity of leachable components. Survivability of HDF in all concentrations (3.15%, 6.25%, 12.5%, 25%, 50%, 100%) of extraction from the IPV devices after 24 h is 93%–106%, which is similar to nontoxic control results from encapsulations-only (96%–109%) and glass ($\approx$100%, $\approx$0.16 mm, Marienfeld-superior). In contrast, survivability of HDF in 25% and higher concentrations of extraction from a control (0.1% zinc diethyl-dithiocarbamate in polyurethane film) dropped down to $\approx$3%. Splenocytes, immune cells from a hairless mouse, also survives well ($\approx$102%) when they are directly exposed to the IPV devices for 24 h (Figure S11, Supporting Information). Direct measurements of arsenic from a new PDMS layer and from the outermost front and back encapsulation layers (PDMS, size $\approx$7 mm $\times$ 7 mm) of the IPV device (Figure 3g) using an inductively coupled plasma quadruple mass spectrometer (ICP-QMS) 8 weeks after implantation detected the following amounts: $\approx$0.02, $\approx$0.12, and $\approx$0.03 µg, respectively. For a human, these amounts are much lower than the daily intake from breathing air ($\approx$0.6 µg)[56] or from drinking water ($\approx$20 µg),[57] indicating that no significant amount of arsenic is leached to the encapsulation layers.

Subdermal IPV devices can power various types of assistive electronics in a body. **Figure 4**a shows an example, subdermally implantable flexible pacemaker integrated with the IPV device and rechargeable battery (6.5 µAh at voltage range from 2 to 3.3 V, Seiko). See details for circuit diagram of the pacemaker system in Figure S12 of the Supporting Information. Open-circuit voltage (V_{oc} = 4.6 V) of the IPV device is high enough to operate the custom-built pacemaker (V = 1.5–2 V, I = 76–105 µA). The simple pacemaker does not have a housekeeping mode and the power requirement is for pacing only. The implanted IPV device ($\eta \approx$10.7%) can supply about $\approx$195 µA of current to the pacemaker. The self-powered pacemaker is flexible and subdermally implantable (Figure 4b). Figure 4c shows the subdermally implanted pacemaker powered by the IPV device under the skin of a live hairless mouse. To regulate heart beating, electrical impulses are delivered to the heart muscles by contacting the right atrium (RA) and left ventricle (LV) with the leads from the pacemaker(Figure 4d). Figure 4e shows electrical impulses (V_p = $\approx$1.5 V, duty cycle = $\approx$3 Hz, pulse width = $\approx$5 ms) from the implanted pacemaker. When light source is available (illumination on, $\approx$AM1.5G), the impulses (black line) are generated with power from the IPV device under the skin. Even without light source available (illumination off), the impulses (blue line) still continues because the subdermally implanted pacemaker can be powered with a battery that is recharged by the IPV device. See details for characteristics of the battery integrated with IPV device in Figure S13 of the Supporting Information. Under bradycardia state with chest open, the heart rate of the mouse is about 1 Hz as shown with the ECG signals in Figure 4f. When the external illumination is on, the subdermally implanted pacemaker powered by the IPV device regulates the heart rate (black line) in $\approx$3 Hz as shown in Figure 4g. With illumination is off, regulation of the heart rate

Materials Views
www.MaterialsViews.com

ADVANCED
HEALTHCARE
MATERIALS
www.advhealthmat.de

COMMUNICATION

Figure 3. Effects by additional coverings and biocompatibility assessments. a) Schematic illustration of a sunscreen layer (up) and optical image of a hydrocolloid bandage (down) on the skin over the IPV device. b) Energy conversion efficiencies measured in vivo (blue bar) and calculated, c) based on transmittance (mean ± SEM, n = 7), with additional coverings. A layer of sunscreen does not affect the conversion efficiency. d) Images of histological sections from three different skin tissues 4 weeks after implantation: with no implant (left), with the IPV device including encapsulation layers (middle), and with encapsulation layers lacking solar microcells (right). e) Histologic scores of fibrosis and PMN cells, counted by thicknesses of fibrosis and by number of PMN cells, respectively. The histologic scores of fibrosis and PMN cells in the tissues surrounding the IPV device are similar to the scores of the encapsulation layers only. f) Survivability of human dermal fibroblast (HDF) cells for 24 h, in the diluted extracts from the IPV device, encapsulation layer only, glass and 0.1% zinc diethyldithiocarbamate (ZDEC) polyurethane (PU) film. Survivability of the HDF cells in the extract from the IPV device is similar to survivability in the extracts from the biocompatible materials, such as encapsulation-only or glass. The survivability reduces drastically at higher concentration (>25%) of the extract from ZDEC-PU film that is known to be toxic. g) An image of an IPV device covered by subcutaneous cellular tissues. Inset: separation of the outmost front and back encapsulation layers (PDMS) from the IPV device. h) Amounts of arsenic measured by inductively coupled plasma quadruple mass spectrometer (ICP-QMS), from new PDMS, front and back encapsulations (size ≈7 mm × 7 mm) 8 weeks after implantation are ≈0.02, ≈0.12, and ≈0.03 µg, respectively. These amounts are much lower than the daily intake from breathing air or from drinking water by a person.

(blue line) continues because the pacemaker is still powered by the rechargeable battery. Slight modification of the circuits can generate impulses and pace the heart rate in different frequencies (1, 3, and 5 Hz, Figure S14, Supporting Information).

Other examples powering fully implanted electronics (LEDs) with the fully implanted IPV device and rechargeable battery in live hairless mice confirm feasibility of the concept (Figure S15, Supporting Information).

Generating electricity within the body allows implantable electronic devices to be more sustainable. Figure 4h shows the simulated capacity of a battery (Sigma 213 Lithium-Iodine, 830 mAh) used in a commercially available pacemaker that is charged with an IPV device that has a charging efficiency of 85%[58] within the body. The standard pacemaker consumes about 284 µAh per day by assuming the battery is depleted in 8 years without charging (blue squares, Figure S16, Supporting Information). Under ideal circumstances (AM1.5G illumination (100 mW cm^{-2})), charging the battery with an IPV device ($\eta \approx 8.2\%$) for 126 min each day should provide enough energy to operate the pacemaker indefinitely. It should be
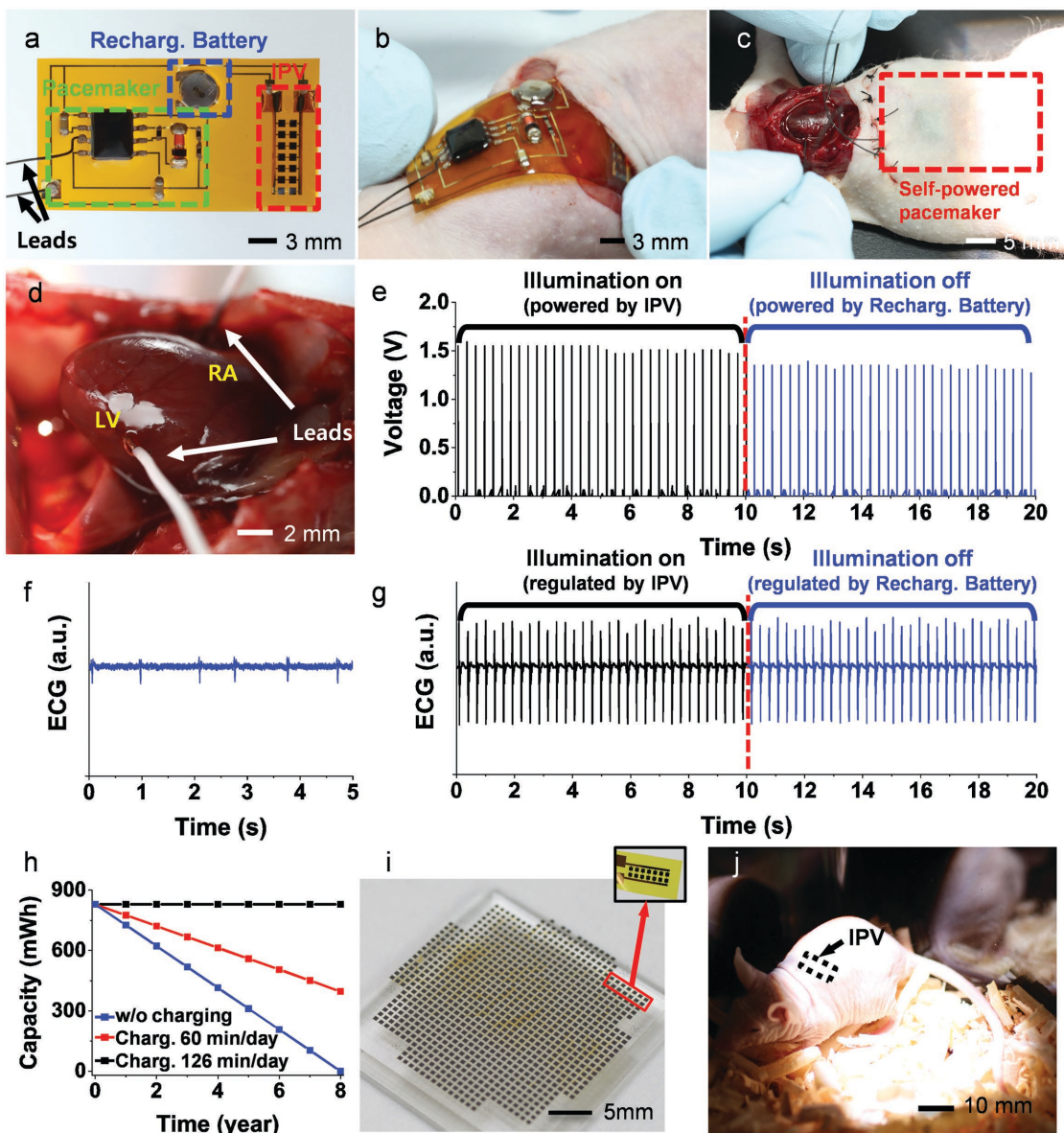
Figure 4. Subdermally implantable self-powered flexible pacemakers. a) Optical image of a flexible cardiac pacemaker integrated with the IPV device and a rechargeable battery. b) The self-powered pacemaker is flexible and subdermally implantable. c) The subdermally implanted pacemaker with energy generation and storage. The IPV device powers the pacemaker and recharges the battery in a live mouse. d) The heart of the live hairless mouse. The leads from the implanted self-powered pacemaker contact the right atrium (RA) and left ventricle (LV) of the heart. e) Output impulses ($\approx$3 Hz) from the subdermally implanted self-powered pacemaker powered by the IPV device under the skin. With illumination on (black line, under AM1.5G), the IPV device power the pacemaker and stores energy to the rechargeable battery. With illumination off (blue line), the rechargeable battery powers the pacemaker with the stored energy. f) ECG signals ($\approx$1 Hz) of the mouse under bradycardia state. g) ECG signals ($\approx$3 Hz) regulated by the self-powered pacemaker. The heart beats are regulated to be $\approx$3 Hz even with illumination off (blue line). h) Simulated capacity of a battery (Sigma 213 Lithium-Iodine, 830 mAh) used in a implanted pacemaker. Under ideal circumstances (AM1.5G illumination (100 mW cm^{-2})), charging the battery with an IPV device ($\eta \approx 8.2\%$) for 126 min a day should provide enough energy to operate the pacemaker indefinitely. i) The IPV device is scalable to provide more power in bodies. Inset: An IPV device next to a dime (radius: 8.95 mm). j) Relative scale of the IPV device implanted in a live hairless mouse model.

www.MaterialsViews.com

ADVANCED
HEALTHCARE
MATERIALS

www.advhealthmat.de

COMMUNICATION

noted that rechargeable battery life could be a limiting factor as the batteries lose a capacity with repetitive charging-loading cycles. The IPV device under human skin is also expected to generate less electrical power because human skins[59] are twice thicker than mice skin. There are also many other factors that may affect negatively to the power output under in real life conditions[33,34] such as lower irradiation intensity indoor, clouds outdoor, hair, skin pigmentation, clothes covering the skin over the IPV devices, incident angles depending on the sites of implantation and extra electronics including a maximum power point tracker that consumes harvestable energy. Thermal safety to surrounding tissues is also an important consideration in determining exposure time. The connecting wires between the IPV device, rechargeable battery, and pacemaker should be short if possible, to reduce possibilities of energy loss by a resistance or damage in the wires. However, IPV devices also have the distinct advantage of being scalable to reduce daily charging time. The IPV device reported here only makes use of a small area (total active area: 6.8 mm^2) of a wafer as shown in Figure 4i. Depending on power requirements of pacemakers, the number or size of the solar microcells are adjustable. Figure 4j shows the relative scale of the IPV device that was implanted into the mouse model.

In summary, we have developed a practically feasible technology for powering in vivo medical devices using available photovoltaic and energy storage technologies. The IPV device reported here requires only simple dermatological surgery and readily generated enough power to operate currently available implants, such as pacemakers. Depending on energy requirements of implants, the short-circuit current, open-circuit voltage, and the output power can be easily adjustable (or scalable) by simply changing interconnections or by adding more solar microcells. More sophisticated encapsulations or lateral designs with other types of photovoltaic materials should lead to further improvements in biocompatibility and durability. Solving electrical energy related problems in a body would accelerate the development of many more types of implantable electronic devices to monitor or assist internal organs.

Experimental Section

Preparation of Implantable Photovoltaic Devices: We prepared the dual junction (GaInP: bandgap ≈1.8 eV, GaAs: bandgap ≈1.4 eV) solar microcells were prepared by wet chemical etching (HCl, 35%, H3PO4, 85%, OCI) to define the shape (lateral type, size: 760 μm × 760 μm, thickness: 6 μm), and by metal deposition (Ti: 20 nm, Au: 60 nm) to form top (size: 700 μm × 40 μm) and bottom (size: 760 μm × 40 μm) contacts with an electron beam evaporator (deposition speed ≈0.5 Å s^{-1}, pressure ≈2 × 10^{-6} Torr). We separated the microcells from the original wafer with an elastomeric stamp (PDMS, polydimethylsiloxane, thickness ≈3 mm) and transfer-printed onto a PI film (polyimide, ≈12.5 μm) with an aid of an adhesive layer (SU-8, ≈2 μm, Microchem). Sputtering and lifting off metal layers (Ti: 20 nm, Au: 300 nm) formed interconnects to connect seven columns in parallel and two rows in series. We encapsulated the top of the interconnected devices with optically transparent, biocompatible layers of SU-8 (thickness ≈2 μm) and NOA (≈23 μm, Norland optical adhesives, Norland Products). To prevent excessive strain or even breakage in the solar microcells and metal interconnects. We determined the thicknesses of the encapsulation layers to position the neutral mechanical plane close to the inorganic

devices and metal interconnects, as reported previously.[60,61] As a final step, we encapsulated the devices with layers of PDMS (100–200 μm, biocompatible) on top and bottom to minimize exchange of any substances between the devices and live bodies. More details with schematic illustration are in the Supporting Information (Figure S1, Supporting Information). For in vivo measurements or demonstrations, insulated copper wires (radius: 0.1 mm), registors, capacitors, timers (IKSEMICON) or rechargeable batteries (Seiko Instruments) were mounted on the interconnects using a layer of conductive epoxy before forming the encapsulation layers.

Implantation of the IPV Devices: We implanted the IPV device into a live hairless mouse (SKH1-Hr^{hr}, 8–12 weeks old, ≈30 g) for in vivo study. Use of the animal in this study was approved by GIST IACUC (GIST-2014-48). The surgery started with intraperitoneal injection of anesthetic (300 μL), mixture of ketamine (70 mg kg^{-1}, Ketamin 50) and xylazine (7 mg kg^{-1}, Rompun), to put the mouse under general anesthesia. After sterilizing dorsal skins with povidone Iodine (10%) and ethanol (70%), we made a straight paravertebral incision (≈1 cm) on the back. We made the space in adipose tissue layers, inserted the IPV device and performed wound closure with sutures.

In Vivo Measurements of Electrical Properties: For in vivo measurements only, the implanted devices were connected to the external measurement systems with insulated copper wires passing through the skin although the implanted devices did not require any electrical lines passing through the skin to function in the body. The wires were taken out of the body through the skin during the implanting surgery or after healing the incision for 1–2 weeks after the surgery. After administering general anesthetic (300 μL), we measured electrical properties, e.g., current–voltage characteristics, power density, etc., of the implanted devices, with a source meter unit (2400 SourceMeter, Keithley Instrument) under a solar simulator (Sol3A Class AAA solar simulator, Oriel Instruments) with standard spectrum (AM1.5G) and irradiation intensity (100 mW cm^{-2}). The performance for charging (voltage vs time) the rechargeable battery with current supplied by the IPV devices was characterized with source/measure unit (B2902A, Keysight technologies) under irradiation by a solar simulator (AM1.5G, LCS-100, Oriel Instruments).

Measurements of Optical Properties: Optical properties of the skins of the hairless mouse were characterized with a pair of double-integrating spheres (Avasphere-30, port diameter: 6 mm, Avantes), a set of ICCD (intensified charge coupled device) spectrometers (PI-MAX3, Princeton Instruments), a light lamp (Avalight-HAL, Avantes), and optical fibers (BFL37-1000, Thorlabs). The integrating spheres are designed to collect all the scattered lights after reflection and transmission. The ICCD spectrometers acquire reflected or transmitted light at the interval of 0.1 nm in the range from 400 to 950 nm. We averaged 20 sets of the data measured at the same position for 100 ms in every 1 s. The spectral transmittance of the skin was then calculated by dividing the average intensity by the maximum intensity measured without the skin. We made skin flaps, not completely removed from hairless mice under general anesthesia, with similar methods when implanting the IPV devices. We isolated the skin flaps (≈1.5 cm × 1.5 cm) completely just before loading (within ≈10 min) between the integrating spheres to acquire optical properties close to the live ones. The detectors in the upper and lower integrating sphere collect reflected light on the skin and transmitted light through the skin, respectively. More details are in the Supporting Information (Figure S6).

In Vivo Biocompatibility Study: Hairless mice (SKH1-Hr^{hr}, 6–8 weeks old female) acclimatized for at least 1 week before the experiments, fed Purina Chow diet and water ad libitum in standard conditions of 12 h light/12 h dark cycle in 24 ± 2 °C and 50 ± 10% relative humidity. The implants and surrounding tissues were gently excised from the mice sacrificed with CO_2 asphyxiation. The tissues were fixed in 4% paraformaldehyde, embedded in paraffin, cut into sections (≈5 μm). The sections were stained with hematoxylin and eosin (H&E) and Accustain trichrome stain (Masson) kit (Sigma). A board certified dermatologist inspected, scored, and analyzed the histologic slides in blinded fashion. Fibrosis (sections N = 9) and polymorphonuclear cells (sections N = 7) were scored by thicknesses and number of the cells, respectively, with

COMMUNICATION

optical microscope images from randomly selected regions in high power field (HPF, ×400). All data are presented as median (25%–75% interquartile range). The identical experiments repeated three times. Statistical analysis was conducted with Kruskall Wallis test and Mann-Whitney U test (two-tailed distribution) by using IBM SPSS Statistics 19.0. Statistical significance was ascribed at $p < 0.05$.

In Vitro Biocompatibility Study: Human dermal fibroblasts (HDF) were sub-cultivated and cultured in Dulbecco's Modified Eagle Medium (DMEM) supplemented with 10% (v/v) fetal bovine serum and 1% (v/v) of penicillin/streptomycin solution (Gibco/Invitrogen, Carlsbad, CA, USA) in an incubator at 37 °C, 5% CO_2, and 95% relative humidity. The HDFs (density $\approx 1 \times 10^4$ per well, passages 5–8) seeded and incubated for 24 h in 96 well plate were exposed to various concentrations (undiluted, 75%, 50%, 25%, 12.5%, 6.25%, and 3.125% diluted in media) of extracted solutions for 24 h. The extracted solutions were obtained by immersing the IPV devices, encapsulation layers only, glass slides, ZDEC-PU films in unsupplemented culture media (two samples (each ≈ 1.5 cm $\times 1$ cm) per 2 mL medium) to extract any soluble or leachable constituents at body temperature (37 °C) for 48 h.[53] Splenocytes, nonadherent immune cells, acquired by crushing spleens of SKH1-Hr^{hr} with frosted slides and homogenizing with 70 μm cell strainer (BD Biosciences, USA) were cultured in RPMI-1640 (Hyclone, Logan, UT, USA) supplemented with 10% fetal bovine serum and 1% penicillin/streptomycin solution. Splenocytes were exposed directly to the IPV devices, encapsulation layers only, glass slides, ZDEC-PU films for 24 h. Fibroblasts and splenocytes were incubated for 2 h with addition of 10% Ez-cytox, forming the water-soluble formazan dyes. Especially in splenocytes sample, 300 μL of this formazan solution was collected from each sample and divided into three wells of 96 well plate (100 μL in each well). The survivability of the cells is estimated with absorbance (wavelength: 450 nm, measured by chameleon microplate reader, Hidex, Turku, Finland) of the water-soluble formazan dyes by comparing absorbance of dyes formed from nonexposed cells.

Supporting Information

Supporting Information is available from the Wiley Online Library or from the author.

Acknowledgements

[1] H. G. Mond, A. Proclemer, *PACE – Pacing Clin. Electrophysiol.* **2011**, *34*, 1013.

[2] M. A. Wood, K. A. Ellenbogen, *Circulation* **2002**, *105*, 2136.

[3] X. Wei, J. Liu, *Front. Energy Power Eng. China* **2008**, *2*, 1.

[4] J. A. Potkay, *Biomed. Microdevices* **2008**, *10*, 379.

[5] C. Henry, *Anal. Chem.* **1998**, *70*, 594A.

[6] A. Y. Chow, V. Y. Chow, K. H. Packo, J. S. Pollack, G. A. Peyman, R. Schuchard, *Arch. Ophthalmol.* **2004**, *122*, 460.

[7] T. Someya, T. Sekitani, S. Iba, Y. Kato, H. Kawaguchi, T. Sakurai, *Proc. Natl. Acad. Sci. USA* **2004**, *101*, 9966.

[8] C. Wang, D. Hwang, Z. Yu, K. Takei, J. Park, T. Chen, B. Ma, A. Javey, *Nat. Mater.* **2013**, *12*, 1.

[9] I. R. Minev, P. Musienko, A. Hirsch, Q. Barraud, T. Milekovic, L. Asboth, R. F. Torres, N. Vachicouras, *Science* **2012**, *347*, 159.

[10] V. Gradinaru, F. Zhang, C. Ramakrishnan, J. Mattis, R. Prakash, I. Diester, I. Goshen, K. R. Thompson, K. Deisseroth, *Cell* **2010**, *141*, 154.

[11] T. Kim, J. G. McCall, Y. H. Jung, X. Huang, E. R. Siuda, Y. Li, J. Song, Y. M. Song, H. a. Pao, R.-H. Kim, C. Lu, S. D. Lee, I.-S. Song, G. Shin, R. Al-Hasani, S. Kim, M. P. Tan, Y. Huang, F. G. Omenetto, J. a. Rogers, M. R. Bruchas, *Science* **2013**, *340*, 211.

[12] W. H. Yeo, Y. S. Kim, J. Lee, A. Ameen, L. Shi, M. Li, S. Wang, R. Ma, S. H. Jin, Z. Kang, Y. Huang, J. a. Rogers, *Adv. Mater.* **2013**, *25*, 2773.

[13] A. Zebda, C. Gondran, A. Le Goff, M. Holzinger, P. Cinquin, S. Cosnier, *Nat. Commun.* **2011**, *2*, 370.

[14] L. Halámková, J. Halámek, V. Bocharova, A. Szczupak, L. Alfonta, E. Katz, *J. Am. Chem. Soc.* **2012**, *134*, 5040.

[15] Z. Li, G. Zhu, R. Yang, A. C. Wang, Z. L. Wang, *Adv. Mater.* **2010**, *22*, 2534.

[16] W. Tang, J. Tian, Q. Zheng, L. Yan, J. Wang, Z. Li, Z. L. Wang, *ACS Nano* **2015**, *9*, 7867.

[17] Q. Zheng, B. Shi, F. Fan, X. Wang, L. Yan, W. Yuan, S. Wang, H. Liu, Z. Li, Z. L. Wang, *Adv. Mater.* **2014**, *26*, 5851.

[18] C. Dagdeviren, B. D. Yang, Y. Su, P. L. Tran, P. Joe, E. Anderson, J. Xia, V. Doraiswamy, B. Dehdashti, X. Feng, B. Lu, R. Poston, Z. Khalpey, R. Ghaffari, Y. Huang, M. J. Slepian, J. a. Rogers, *Proc. Natl. Acad. Sci. USA* **2014**, *111*, 1927.

[19] A. Yakovlev, S. Kim, A. Poon, *IEEE Commun. Mag.* **2012**, *50*, 152.

[20] A. K. Ramrakhyani, S. Mirabbasi, M. Chiao, C. M, *IEEE Trans. Biomed. Circuits Syst.* **2011**, *5*, 48.

[21] P. Si, A. P. Hu, S. Malpas, D. Budgett, *Biomed. Circuits Syst.* **2008**, *2*, 22.

[22] J. S. Ho, A. J. Yeh, E. Neofytou, S. Kim, Y. Tanabe, B. Patolla, R. E. Beygui, a. S. Y. Poon, *Proc. Natl. Acad. Sci. USA* **2014**, *111*, 7974.

[23] P. P. Mercier, A. C. Lysaght, S. Bandyopadhyay, A. P. Chandrakasan, K. M. Stankovic, *Nat. Biotechnol.* **2012**, *30*, 1240.

[24] J. Olivo, S. Carrara, G. De Micheli, G. De Micheli, *IEEE Sens. J.* **2011**, *11*, 1573.

[25] M. A. Hannan, S. Mutashar, S. A. Samad, A. Hussain, *Biomed. Eng. Online* **2014**, *13*, 79.

[26] E. Katz, *Bioelectron. Med.* **2015**, *2*, 1.

[27] E. Katz, K. MacVittie, *Energy Environ. Sci.* **2013**, *6*, 2791.

[28] W. Jia, X. Wang, S. Imani, A. J. Bandodkar, J. Ramírez, P. P. Mercier, J. Wang, *J. Mater. Chem. A* **2014**, *2*, 18184.

[29] A. J. Bandodkar, I. Jeerapan, J.-M. You, R. Nuñez-Flores, J. Wang, *Nano Lett.* **2016**, *16*, 721.

[30] A. J. Bandodkar, J. Wang, *Electroanalysis* **2016**, *28*, 1.

[31] K. Mathieson, J. Loudin, G. Goetz, P. Huie, L. Wang, T. I. Kamins, L. Galambos, R. Smith, J. S. Harris, A. Sher, D. Palanker, *Nat. Photonics* **2012**, *6*, 391.

[32] H. Lorach, G. Goetz, R. Smith, X. Lei, Y. Mandel, T. Kamins, K. Mathieson, P. Huie, J. Harris, A. Sher, D. Palanker, *Nat. Med.* **2015**, *21*, 476.

[33] A. Haeberlin, A. Zurbuchen, J. Schaerer, J. Wagner, S. Walpen, C. Huber, H. Haeberlin, J. Fuhrer, R. Vogel, *Europace* **2014**, *16*, 1534.

[34] A. Haeberlin, A. Zurbuchen, S. Walpen, J. Schaerer, T. Niederhauser, C. Huber, H. Tanner, H. Servatius, J. Seiler, H. Haeberlin, J. Fuhrer, R. Vogel, *Hear. Rhythm* **2015**, *12*, 1317.

[35] J. Lee, J. Wu, J. H. Ryu, Z. Liu, M. Meitl, Y. W. Zhang, Y. Huang, J. a. Rogers, *Small* **2012**, *8*, 1851.

[36] K. V. Nemani, K. L. Moodie, J. B. Brennick, A. Su, B. Gimi, *Mater. Sci. Eng. C* **2013**, *33*, 4453.

www.MaterialsViews.com

ADVANCED
HEALTHCARE
MATERIALS

www.advhealthmat.de

COMMUNICATION

[37] USP Class VI NOA 61, https://www.norlandprod.com/UV-news.asp (accessed: 2014).

[38] M. C. Bélanger, Y. Marois, *J. Biomed. Mater. Res.* **2001**, *58*, 467.

[39] M.-H. Wu, J.-L. Lin, J. Wang, Z. Z. Cui, Z. Z. Cui, *Biomed. Microdevices* **2009**, *11*, 265.

[40] S. Cosnier, A. Le Goff, M. Holzinger, *Electrochem. Commun.* **2014**, *38*, 19.

[41] E. Wrzesniewski, S. H. Eom, W. Cao, W. T. Hammond, S. Lee, E. P. Douglas, J. Xue, *Small* **2012**, *8*, 2647.

[42] F. Benavidesa, T. M. Oberyszynb, A. M. VanBuskirk, V. E. Reeved, D. F. Kusewitt, *J. Dermatol. Sci.* **2009**, *53*, 10.

[43] P. Lakshmanan, V. Dixit, M. R. Reed, J. L. Sher, *J. Orthop. Surg.* **2010**, *18*, 85.

[44] N. Safdar, D. Kluger, D. Maki, *Medicine.* **2002**, *81*, 466.

[45] A. Niv, Z. R. Abrams, M. Gharghi, C. Gladden, X. Zhang, *Appl. Phys. Lett.* **2012**, *100*, 1.

[46] J. M. Anderson, A. Rodriguez, D. T. Chang, *Semin. Immunol.* **2008**, *20*, 86.

[47] G. Williams, W. J. Williams, *J. Clin. Pathol.* **1983**, *36*, 723.

[48] J. M. Morais, F. Papadimitrakopoulos, D. J. Burgess, *AAPS J.* **2010**, *12*, 188.

[49] F. Bernerd, C. Vioux, D. Asselineau, *Photochem. Photobiol.* **2000**, *71*, 314.

[50] J. G. Fox, M. T. Davisson, F. W. Quimby, S. W. Barthold, C. E. Newcomer, A. L. Smith, *The Mouse in Biomedical Research*, Academic Press, Cambridge, Massachusetts, USA, **2006**.

[51] K. Lehle, S. Lohn, G. G. Reinerth, T. Schubert, J. G. J. G. Preuner, D. E. D. E. Birnbaum, *Biomaterials* **2004**, *25*, 5457.

[52] J. Wedel, M. Weij, A. S. Oosten, J.-L. Hillebrands, *Lab. Anim.* **2014**, *48*, 338.

[53] G. Park, H. J. Chung, K. Kim, S. A. Lim, J. Kim, Y. S. Kim, Y. Liu, W. H. Yeo, R. H. Kim, S. S. Kim, J. S. Kim, Y. H. Jung, T. Il Kim, C. Yee, J. a. Rogers, K. M. Lee, *Adv. Healthcare Mater.* **2014**, *3*, 515.

[54] B. D. Ratner, *J. Controlled Release* **2002**, *78*, 211.

[55] O. Veiseh, J. C. Doloff, M. Ma, A. J. Vegas, H. H. Tam, A. R. Bader, J. Li, E. Langan, J. Wyckoff, W. S. Loo, S. Jhunjhunwala, A. Chiu, S. Siebert, K. Tang, J. Hollister-Lock, S. Aresta-Dasilva, M. Bochenek, J. Mendoza-Elias, Y. Wang, M. Qi, D. M. Lavin, M. Chen, N. Dholakia, R. Thakrar, I. Lacík, G. C. Weir, J. Oberholzer, D. L. Greiner, R. Langer, D. G. Anderson, *Nat. Mater.* **2015**, *14*, 643.

[56] J. Lodge Jr., *Environ. Sci. Pollut. Res.* **1996**, *3*, 23.

[57] F. Ahmed, I. Chorus, J. Cotruvo, D. Cunliffe, A. M. de Roda Husman, T. Endo, J. K. Fawell, M. Giddings, G. Howard, P. Jackson, S. Kumar, S. Kunikane, Y. Magara, A. V. F. Ngowi, E. Ohanian, C. N. Ong, O. Schmoll, M. Sobsey, *WHO Guidelines for Drinking-Water Quality*, 4th ed., **2011**, WHO Press, Geneva, Switzerland.

[58] L. O. Valøen, M. I. Shoesmith, *Plug-in Hybrid Electric Vehicle Conf. PHEV2007*, Winnipeg, Manitoba, Canada, **2007**, p. 1.

[59] S. Richard, J. de Rigal, O. de Lacharriere, E. Berardesca, J.-L. Leveque, *Photodermatol. Photoimmunol. Photomed.* **1994**, *10*, 164.

[60] D.-H. Kim, J. Viventi, J. J. Amsden, J. Xiao, L. Vigeland, Y.-S. Kim, J. a. Blanco, B. Panilaitis, E. S. Frechette, D. Contreras, D. L. Kaplan, F. G. Omenetto, Y. Huang, K.-C. Hwang, M. R. Zakin, B. Litt, J. a. Rogers, *Nat. Mater.* **2010**, *9*, 511.

[61] J. Yoon, A. J. Baca, S.-I. Park, P. Elvikis, J. B. Geddes, L. Li, R. H. Kim, J. Xiao, S. Wang, T.-H. Kim, M. J. Motala, B. Y. Ahn, E. B. Duoss, J. a. Lewis, R. G. Nuzzo, P. M. Ferreira, Y. Huang, A. Rockett, J. a. Rogers, *Nat. Mater.* **2008**, *7*, 907.